Soft Matter

Accepted Manuscript

This is an *Accepted Manuscript*, which has been through the Royal Society of Chemistry peer review process and has been accepted for publication.

Accepted Manuscripts are published online shortly after acceptance, before technical editing, formatting and proof reading. Using this free service, authors can make their results available to the community, in citable form, before we publish the edited article. We will replace this *Accepted Manuscript* with the edited and formatted *Advance Article* as soon as it is available.

You can find more information about *Accepted Manuscripts* in the Information for Authors.

Please note that technical editing may introduce minor changes to the text and/or graphics, which may alter content. The journal's standard Terms & Conditions and the Ethical guidelines still apply. In no event shall the Royal Society of Chemistry be held responsible for any errors or omissions in this *Accepted Manuscript* or any consequences arising from the use of any information it contains.

ROYAL SOCIETY OF CHEMISTRY

www.rsc.org/softmatter

Soft Matter
CREATED USING THE RSC LaTeX PCCP ARTICLE TEMPLATE – SEE www.rsc.org/electronicfiles FOR DETAILS
PAPER
www. rsc.org/xxxxxx | XXXXXXXX

Using infrared thermography to study hydrostatic stress networks in granular materials

Pawarut Jongchansitto,[ab] Xavier Balandraud,*[b] Michel Grédiac,[b] Clément Beitone,[b] and Itthichai Preechawuttipong[a]

Received Xth XXXXXXXXXX 20XX, Accepted Xth XXXXXXXXX 20XX
First published on the web Xth XXXXXXXXXX 200X
DOI: 10.1039/b000000x

The macroscopic mechanical behaviour of granular materials is governed by microscopic features at the particle scale. Photoelasticimetry is a powerful method for measuring shear stresses in particles made from birefringent materials. As a complementary method, we here identify the hydrostatic stress networks through thermoelastic stress analysis using infrared thermographic measurements. Experiments are performed on two-dimensional cohesionless monodisperse granular materials composed of about 1200 cylinders comprising two constitutive materials. We show that the experimental hydrostatic stress distributions follow statistical laws which are in agreement with simulations performed using molecular dynamics, except in one case exhibiting piecewise periodic stacking. Polydisperse cases are then processed. The measurement of hydrostatic stress networks using this technique opens new prospects for the analysis of granular materials.

Various articles in the literature address the study of the mechanical behaviour of granular materials (GMs) via numerical approaches. These approaches enable us to study in detail the influence of parameters such as particle shape, density, polydispersity, particle elasticity, friction, etc. Although many significant advances have been made using these approaches, there is a lack of experimental data enabling numerical methods to be validated. Some approaches deal with measurements in the bulk, such as X-ray tomography [1,2], magnetic resonance imaging [3,4], radar-based sensing [5] and positron emission particle tracking [6]. Apart from these techniques, the literature mainly concerns two-dimensional (2D) techniques based on optical photography. Concerning the direct observation of stresses, photoelasticimetry is now a common technique used for 2D GMs composed of birefringent materials: see for instance Refs. [7–15] published in the last few years. Basically, photoelasticimetry provides the difference between the principal stresses, which is proportional to the shear stress. As a new approach, we apply here a 2D measurement technique which enables us to obtain the sum of the principal stresses, which is proportional to the hydrostatic stress. Using thermoelastic stress analysis [16–18], we measure stress distributions thanks to thermal images acquired by an infrared (IR) camera. Indeed, when a material is subjected to stress, it produces or absorbs a heat quantity related to its internal energy variation, *i.e.* to the volumetric part of the strain (first invariant of the strain tensor, also named cubic dilatation). This phenomenon is sometimes named thermoelastic coupling or isentropic coupling. The expression of the heat induced by material thermo-dilatability can be deduced from the second derivative of the Helmholtz free energy function with respect to temperature and strain [19]. In the case of an adiabatic evolution and an isotropic material, the temperature change is proportional to the hydrostatic stress change. The advantage is that, contrary to photoelasticimetry, the technique is potentially applicable to all types of constitutive materials, including opaque materials. The hydrostatic stress at the centre of a cylinder being proportional to the sum of the amplitudes of the normal contact forces applied to the cylinder, this quantity can be used as a new indicator to perform comparisons between experiments and simulations.

The procedure is first performed on cohesionless monodisperse GMs subjected to confined vertical compression. 2D media are here prepared by periodically stacking cylinders with a diameter of 10.50 mm. Two base materials are used in order to construct composite GMs: high-density polyethylene (HDPE) and polyoxymethylene (POM). The cylinders are arranged in parallel in a metallic frame placed on a uniaxial testing machine. Three configurations are tested, each one being characterized by a different ratio between the number of POM and HDPE cylinders: 0.54 (sample #1), 1.07 (#2) and 1.83 (#3), see Table 1. The POM and HDPE cylinders are randomly placed in the frame. However, configuration #1 exhibits piecewise periodic stacking, comprising three zones delimited by parallel straight lines like grain boundaries (see Fig. 1a). This configuration is deliberately created to induce a heterogeneous mechanical response at the mesoscopic scale, for the

[a] *Chiang Mai University, Faculty of Engineering, Department of Mechanical Engineering, 239 Huay Kaew Rd., Chiang Mai 50200, Thailand.*
[b] *Clermont Université, Institut Pascal, UMR CNRS/UBP/IFMA 6602, Campus de Clermont Les Cézeaux, BP 80026, 63171 Aubière cedex, France. Fax: +33 473288100; Tel: +33473288089; E-mail: xavier.balandraud@ifma.fr*

Soft Matter Accepted Manuscript

Table 1 Percentage P_0 of cylinders exhibiting hydrostatic stresses greater than the mean value. Values are given considering all the cylinders independently of their constitutive material (column A), and considering only the POM or only the HDPE cylinders (columns B and C, respectively)

	Numbers of cylinders	A Percentage P_0 of cylinders with stress greater than the mean value		B Same, for POM cylinders only		C Same, for HDPE cylinders only	
	HDPE:POM (ratio)	Experiment	Simulation: mean (standard deviation)	Experiment	Simulation	Experiment	Simulation
#1	807:435 (1:0.54)	39.6%	47.4% (1.3%)	41.4%	48.5% (2.1%)	41.9%	49.0% (2.8%)
#2	597:638 (1:1.07)	45.0%	43.5% (1.0%)	49.4%	47.2% (2.1%)	48.3%	46.3% (3.8%)
#3	436:799 (1:1.83)	44.2%	48.1% (2.4%)	43.7%	48.1% (2.3%)	46.4%	41.8% (3.2%)

first illustration of our technique. Each GM is compressed (here up to -60 kN) prior to testing, in order to reach static equilibrium. As required for a thermoelastic stress analysis, force-controlled cyclic loading is then applied (here between -6 kN and -60 kN at a frequency f of 3 Hz). An IR camera is used to capture the temperature fields on the front face of the cylinder network during this cyclic loading. A Cedip Jade III-MWIR camera featuring 320×240 pixels is employed here with an acquisition frequency of 148 Hz. The pixel size on the measurement plane is equal to 1.60 mm. By considering the thermal diffusivity D of POM and HDPE materials, the order of magnitude of the thermal diffusion length $\sqrt{D/\pi f}$[20] is equal to 0.1 mm for both materials, which is much lower than the cylinder diameter and the pixel size in the measurement plane. Note that the choice of the loading frequency results from a compromise between desired thermal diffusion length and testing machine capability. A Fourier analysis is carried out at each pixel to extract the amplitude ΔT of the temperature oscillation. The relationship between ΔT and the amplitude of the sum of the in-plane principal stresses σ_1 and σ_2 is given by $\Delta T = A(\sigma_1 + \sigma_2)$. Cylinder cross sections are not painted black in order to distinguish POM and HDPE in optical images and find their centres and diameters, which are used in the simulations. As thermal emissivity is not guaranteed to be close to one, coefficient A is preliminarily identified from uniaxial tensile tests on non-painted rectangular sheets: 0.0150 K/MPa for POM and 0.0258 K/MPa for HDPE. The hydrostatic stress σ (given by $\sigma = \Delta T/3A$) is obtained for each cylinder, using the value of A corresponding to the cylinder's material. In practice, we measure the mean hydrostatic stress at the centre of each cylinder over a zone of 3×3 pixels. Similarly to what is done for contact forces, values are then normalised. The normalised hydrostatic stresses σ_{norm} are obtained by dividing by the mean value over the whole GM.

In Fig. 1b, we show the field of σ_{norm} for sample #1. As a consequence of the piecewise periodic stacking, we observe a specific stress pattern which is mainly composed of two zones separated by an oblique line. For comparison purposes, Fig. 1c shows the contact force network obtained using a molecular dynamics simulation[21] carried out on a model of this GM. The method relies on an explicit algorithm in which the particles are considered as rigid bodies with non-conforming surfaces. It is based on a predictor-corrector scheme with Gear's set of corrector coefficients in order to integrate Newton's equations of motion. The contact stiffnesses used in this simulation are initially identified from elementary experiments on a cylinder of each constitutive material. The normalised hydrostatic stresses are obtained from the simulated contact forces by dividing the sum of the amplitudes of the normal contact forces on each cylinder by the mean value over the GM: see Fig. 1d. From a qualitative point of view, a good agreement is observed between experiments and simulations. As expected, some differences can be noted, such as the high stress zone in the bottom-left corner, which is not obtained experimentally. It can also be noted that local fluctuations are more heterogeneous in the experiment than in the simulation. These differences can be explained by local fluctuations of microscopic features and by the difficulty in retrieving the precise location of each cylinder to be placed in the model.

In Fig. 2a, we show the experimental stress fields for samples #2 and #3. The two fields share some common features, such as lines of high stress along directions inclined by $\pm 30^o$ with respect to the vertical, which can be related to a triangular contact network. As a comparison between experiments and simulations, let us first consider a macroscopic output: the percentage P_0 of cylinders exhibiting stresses higher than the mean value ("strong" network). Table 1 presents the percentages obtained over the whole GMs (column A). Interestingly, all the experimental percentages are lower than 50%, which is similar to what is usually estimated for contact forces using numerical approaches[22]. The percentages obtained from our simulations are also given in Table 1. For the three samples, thirty simulations are performed by placing the POM and HDPE cylinders randomly in order to obtain a mean value and a standard deviation for the output data. This enables us to provide generic data on our simulations. Column A in Table 1 shows that the experimental percentages of cylinders exhibiting stresses higher than the mean values over the whole GM

Soft Matter Accepted Manuscript

This journal is © The Royal Society of Chemistry [year]

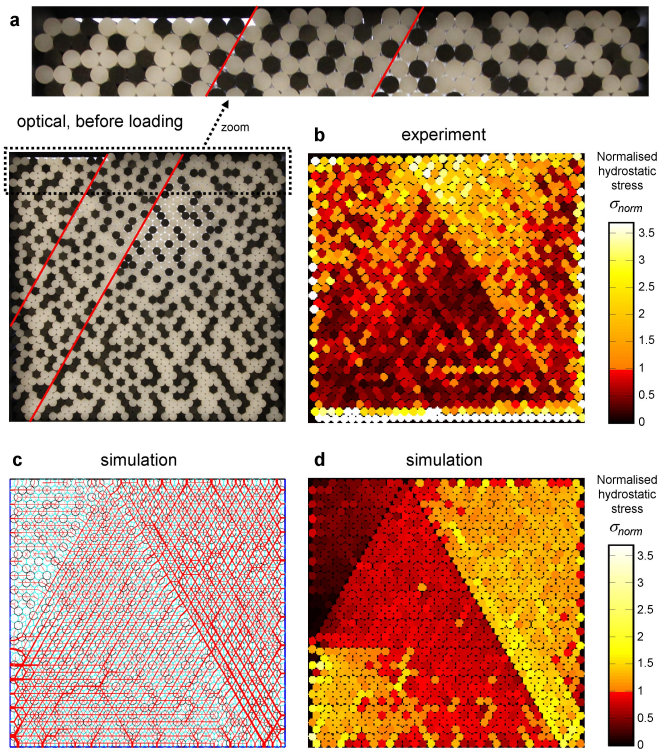

Fig. 1 Results obtained for monodisperse granular material #1, exhibiting piecewise periodic stacking. a) Optical image before loading. b) Experimental field of normalised hydrostatic stresses σ_{norm}. c) Simulated contact force network; the width of the red lines is proportional to the force amplitude. d) Field of σ_{norm} derived from the simulated contact force network

are very close to the simulated ones, except for sample #1. Similar comments can be made when considering only POM or only HDPE cylinders (columns B and C): experimental outputs are close to simulations, within a range of twice the standard deviation. These observations show that simulations are sufficient to extract this macroscopic output data, except for sample #1.

Let us now consider the probability distribution of the stress in the three tested GMs. Fig. 2b presents the experimental probability density function P of σ_{norm} for each sample. We focus only on stresses higher than the mean value, making this choice to limit the effect of the low signal-to-noise ratios in our analysis. Moreover, even if low stresses probably play a role in sustaining strong stress chains, high stresses are interesting, for instance, in understanding the damage in granular materials in terms of particle crushing[23]. As for the case of contact forces in Ref.[24] for instance, we propose to define these distributions using exponential laws: $P = P_0 \exp(-\beta(\sigma_{norm} - 1))$, where the coefficient β characterizes the exponential decay ($\beta > 0$). This type of distribution is confirmed experimentally here, even for sample #1, as can be observed in Fig. 2c, where the distributions are plotted with a semi-logarithmic graph. Values for β are identified by mean square approximation from the curves in Fig. 2b. It can be seen in Table 2 that the values of β are quite similar for samples #2 and #3. They are in good agreement with numerical results (within a range of a few standard deviations). It is noted in the literature that simulated contact force distributions may be independent of some parameters, such as particle size distribution in the case of GMs composed of one type of constitutive material[24]. A similar property is found here experimentally for hydrostatic stresses in samples #2 and #3, which differ in terms of the ratio between the numbers of POM and HDPE cylinders. Let us now analyze the distribution for sample #1. Although the mesoscopic stress pattern is composed of distinct zones (see Fig. 1b), an exponential decay is measured here, too: see the square symbols, which are linearly aligned in Fig. 2c. Although the distribution for sample #1 obtained by our simulations is not really of an exponential type (non-linear curve in semi-logarithmic plotting, curve not reported here), the value of β extracted from mean square approximation provides a first-order indicator of the decay which characterizes the simulated stress distribution. Table 2 shows that the experimental decay is much lower than the simulated one (*e.g.* 0.70 as opposed to 1.62 for the data over the whole GM, see column A). As noted in Ref.[25], although the numerous models which have been developed for GMs are based on different mathematical structures and microscopic assumptions, they often share common results in terms of contact force distribution. The present experimental result for sample #1 thus constitutes a good candidate for a benchmark of models in terms of the stress distributions which can be extracted from simulations. Addressing this issue is however out of the scope of the present experimental study.

The results obtained here can be used for instance to provide assistance in the design of new GMs. Composite GMs can be built by mixing particles with different properties in terms of size, geometry, thermophysical properties, cost, ease of supply, etc. Two sets of properties can be represented by the HDPE and POM polymers, the latter playing the role of reinforcement: +300% in stiffness, +400% in strength and +50% in cost compared to the former. To prevent particle crushing, we propose to use coefficient β as an indicator of hydrostatic stress amplification with respect to the mean stress level. The lower the value of β, the worse the configuration, in the sense that there is a higher probability of reaching significant hydrostatic stress. The objective is then to design a GM using two criteria: quantity of POM and level of stress amplification. Five polydisperse samples are added to the analysis; see Table 3 and Fig. 3 in which coefficient β is the slope of the linear regression (semi-logarithmic plot) of the probability density function P as a function of normalised hydrostatic stresses

Soft Matter Accepted Manuscript

Table 2 Coefficient β characterizing the distribution law for hydrostatic stresses greater than the mean value

	A for all cylinders		B for POM cylinders only		C for HDPE cylinders only	
	Experiment	Simulation: mean (standard deviation)	Experiment	Simulation	Experiment	Simulation
#1	0.70	1.62 (0.14)	0.78	1.62 (0.18)	0.84	1.79 (0.22)
#2	1.32	1.08 (0.06)	1.58	1.69 (0.21)	1.53	1.73 (0.38)
#3	1.26	1.13 (0.11)	1.32	1.62 (0.32)	1.43	1.06 (0.22)

Table 3 Comparison between different granular materials

	Diameter ratio $\frac{D_{POM}}{D_{HDPE}}$	Number ratio $\frac{N_{POM}}{N_{HDPE}}$	Surface in dm^2 POM	Surface in dm^2 POM + HDPE	β
#1	1	0.54	3.77	10.70	0.70
#2	1	1.07	5.52	10.70	1.32
#3	1	1.83	6.92	10.70	1.26
#4	1.6	0.91	7.06	10.17	0.94
#5	1.6	0.39	5.05	10.21	0.94
#6	1.6	1.24	7.71	10.22	0.78
#7	3.0	0.37	7.95	10.40	0.58
#8	3.0	0.18	6.45	10.41	0.79

σ_{norm} in the strong network. Sample #7 is the worst: it has the largest quantity of POM and the highest level of stress amplification ($\beta = 0.58$). Monodisperse samples #2 and #3 minimise the stress amplification level ($\beta = 1.32$ and $\beta = 1.26$, respectively). However, obtaining perfect periodic stacking requires the placement of the cylinders one after another. Filling the frame without caution leads to piecewise periodic stacking, as in sample #1, and thus to an increase in stress amplification ($\beta = 0.70$ for sample #1). Sample #5 is the best compromise here within the tested cases. The proposed experimental approach is complementary to numerical approaches used in obtaining design rules. The importance of modelling the shape of railway ballast particles was for instance underlined in Ref.[26]; this parameter could be also studied with our experimental approach. Indeed we are now in a position to test more complex shapes for 2D grains.

The applicability of the technique to other constitutive materials, such as metallic powders or geotechnical materials, depends on the value of coefficient A and on the camera measurement resolution, commonly referred to as Noise Equivalent Temperature Difference (NETD) in the supplier datasheet. The Fourier analysis used to estimate the temperature amplitude ΔT of the oscillating thermal signal can be seen as a filtering process. This leads to a significant improvement of the measurement resolution. In the current work, this procedure enables us to achieve a resolution for ΔT of an order of magnitude of 1 mK whereas the NETD of the camera is equal to 20 mK. The order of magnitude of coefficient A is given by the ratio $\alpha T_0/\rho C$, where ρ is the density, C the specific heat, α the coefficient of thermal expansion, and T_0 the mean temperature (in Kelvin) at the material point during the cycles[16–18]. We can now consider two cases which are different from polymeric materials. For aluminium alloys and granitoid rocks at ambient temperature $T_0 \approx 300$ K, we have $A \approx 3$ mK/MPa and $A \approx 1$ mK/MPa respectively (see Refs.[27–29] for the material parameters in the latter case). Thus a hydrostatic stress of 100 MPa for instance leads to a temperature change of 300 mK and 100 mK respectively for aluminium alloys and granitoid rocks, which is much higher than the measurement resolution of ΔT. Obviously, the stress level depends on the considered application and these numerical values only provide orders of magnitude.

As a conclusion, the technique which is proposed here opens new prospects for the analysis of granular materials. First, it should be recalled that it is based on a property shared by all materials, thus potentially allowing us to test any type of material in the future, including real geotechnical constitutive materials. Second, in the case of sands or powders with a huge number of particles, mesoscopic hydrostatic stress fields could be identified. Measurements averaged over one pixel could be used to estimate the changes in internal energy of representative elementary volumes (thermoelastic response is related to internal energy change). This may open prospects for homogenisation in granular materials from experimental energetic quantities. Finally, the technique could easily be adapted to reveal hydrostatic stress paths due to shocks, for which adiabatic conditions are achieved (due to the large difference between the shock duration and the characteristic time of thermal diffusion in the material). The field of temperature changes just after the shock would provide the hydrostatic stress path via simple multiplication by coefficient A. As a consequence, no complex image processing would be necessary, considerably reducing the processing time compared to any other method.

Acknowledgements. The authors gratefully acknowledge the Thailand Research Fund through the Royal Golden Jubilee Ph.D. Program (Grant No. PHD/0159/2552) and the French Embassy in Thailand for their support during this research.

Soft Matter Accepted Manuscript

This journal is © The Royal Society of Chemistry [year]

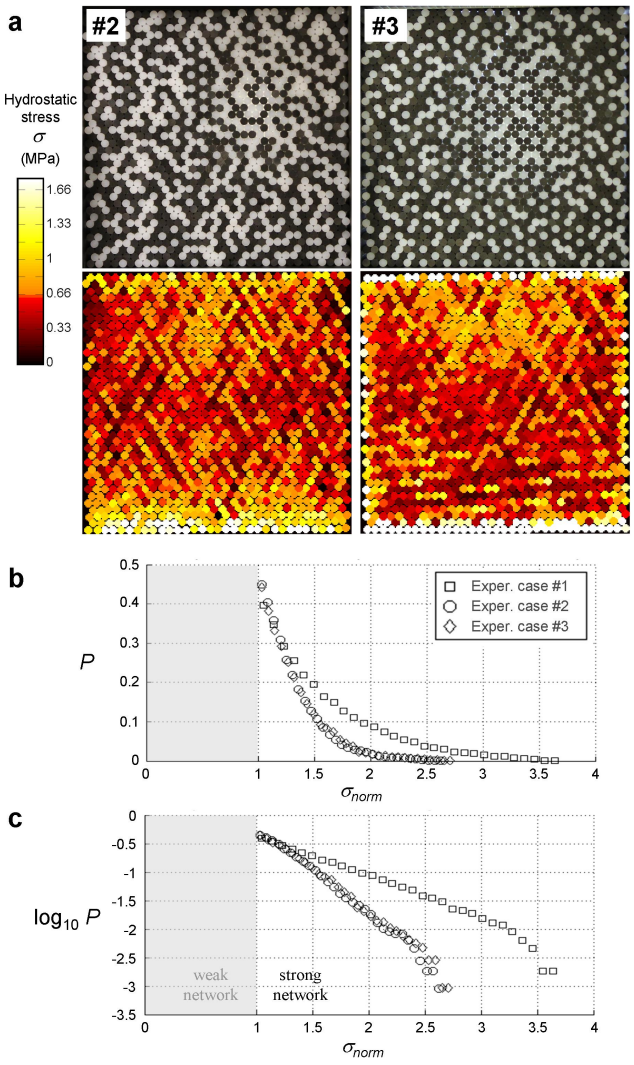

Fig. 2 Experimental results obtained for monodisperse granular materials #2 and #3 exhibiting different POM and HDPE cylinder ratios. a) Top: optical images; bottom: hydrostatic stress field. b) Probability distribution P of normalised hydrostatic stresses σ_{norm} higher than one. c) The same with semi-logarithmic plots. In both graphs, sample #1 is added for comparison purposes

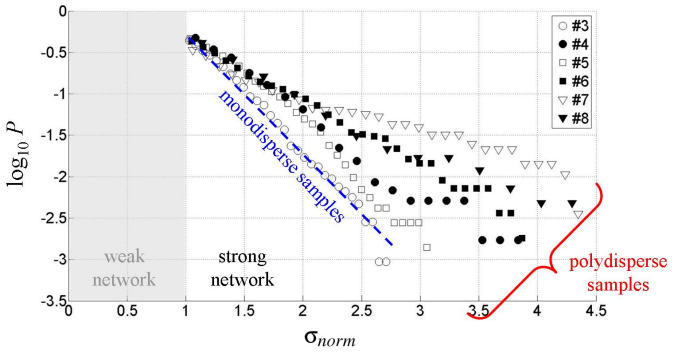

Fig. 3 Probability density function P for various samples

References

1 H. Wolf, D. Konig and T. Triantafyllidis, *J. Struc. Geol.*, 2003, **25**, 1229–1240.
2 S. A. Hall et al., *Geotechnique*, 2010, **60**, 315–322.
3 M. Nakagawa, S. A. Altobelli, A. Caprihan, E. Fukushima and E. K. Jeong, *Exp. Fluids*, 1993, **16**, 54–60.
4 L. Sanfratello, E. Fukushima and R. P. Behringer, *Granular Matter*, 2009, **11**, 1–6.
5 K. M. Hill et al., *Granular Matter*, 2010, **12**, 201–207.
6 D. J. Parker, A. E. Dijkstra, T. W. Martin and J. P. K. Seville, *Chem. Eng. Sci.*, 1997, **52**, 2011–2022.
7 J. Zhang, T. S. Majmudar, M. Sperl and R. P. Behringer, *Soft Matter*, 2010, **6**, 2982–2991.
8 D. Bigoni and G. Noselli, *Eur. J. Mech. A-Solids*, 2010, **29**, 291–298.
9 J. Zhang, T. S. Majmudar, A. Tordesillas and R. P. Behringer, *Granular Matter*, 2010, **12**, 159–172.
10 D. M. Wood and D. Lesniewska, *Granular Matter*, 2011, **13**, 395–415.
11 D. Lesniewska and D. M. Wood, *Geotechnique*, 2011, **61**, 605–611.
12 P. Guo, *Acta Geotechnica*, 2012, **7**, 41–55.
13 J. Estep and J. Dufek, *J. Geophys. Res.-Earth Surface*, 2012, **117**, F01028.
14 L. Zhang, S. X. Cai, Z. P. Hu and J. Zhang, *Soft Matter*, 2014, **10**, 109–114.
15 C. Coulais, R. P. Behringer and O. Dauchot, *Soft Matter*, 2014, **10**, 1519–1535.
16 J. M. Dulieu-Barton and P. Stanley, *J. Strain Anal. Eng. Des.*, 1998, **33**, 93–104.
17 G. Pitarresi and E. A. Patterson, *J. Strain Anal. Eng. Des.*, 2003, **38**, 405–417.
18 R. J. Greene, E. A. Patterson and R. E. Rowlands, in *Springer handbook of experimental solid mechanics*, ed. W. Sharpe Jr, Springer, New York, 2008, ch. 26 Thermoelastic Stress Analysis, pp. 743–768.
19 J. C. Batsale, A. Chrysochoos, H. Pron and B. Wattrisse, in *Full-field measurements and identification in solid mechanics*, ed. M. Grédiac and F. Hild, ISTE Ltd, London, 2013, ch. 16 Thermographic analysis of material behavior, pp. 439–467.
20 S. Offermann, J. L. Beaudoin, C. Bissieux and H. Frick, *Exp. Mech.*, 1997, **37**, 409–413.
21 I. Preechawuttipong, R. Peyroux, F. Radjai and W. Rangsri, *J. Mech. Sci. Technol.*, 2007, **21**, 1957–1963.
22 F. Radjai, D. E. Wolf, M. Jean and J. J. Moreau, *Phys. Rev. Lett.*, 1998, **80**, 61–64.
23 H. Arslan, G. Baykal and S. Sture, *Granular Matter*, 2009, **11**, 87–97.
24 F. Radjai, M. Jean, J. J. Moreau and S. Roux, *Phys. Rev. Lett.*, 1996, **77**, 274–277.
25 T. S. Majmudar and R. P. Behringer, *Nature*, 2005, **435**, 1079–1082.
26 M. Lu and G. R. McDowell, *Granular Matter*, 2007, **9**, 69–80.
27 P. A. Allen and J. R. Allen, in *Basin analysis: principles and application to petroleum play assessment, 3rd edition*, Wiley-Blackwell, Oxford, 2013, ch. 2 The physical state of the lithosphere, pp. 20–50.
28 W. Chesworth, in *Encyclopedia of soil science*, Springer, New York, 2008, ch. H, Heat capacity, pp. 305–307.
29 Z. Li, C. Leung and Y. Xi, in *Structural renovation in concrete*, Taylor & Francis, Oxford, 2009, ch. 4 Conventional repair and strengthening techniques, pp. 147–242.

Soft Matter Accepted Manuscript

Hydrostatic stress networks can be revealed by thermoelastic stress analysis using infrared thermographic measurements

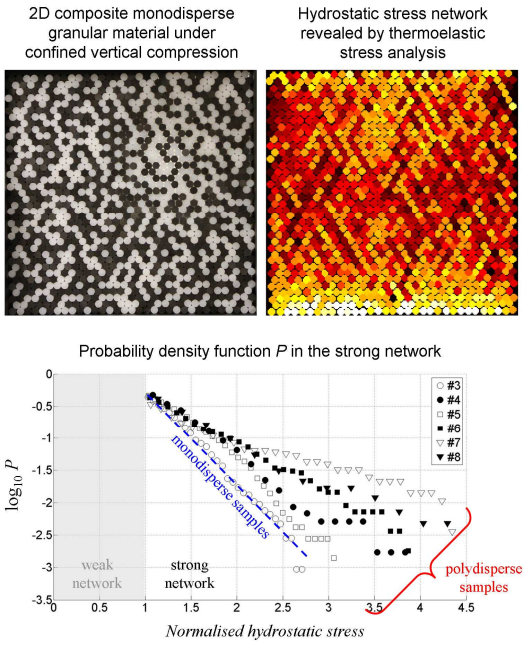

Soft Matter Accepted Manuscript